Environmental Chemistry and Ecotoxicology 7 (2025) 10–18

Contents lists available at ScienceDirect

Environmental Chemistry and Ecotoxicology

journal homepage: www.keaipublishing.com/en/journals/environmental-chemistry-and-ecotoxicology/

Nanostructured bi-metallic biochar: An innovative approach for arsenic (III) removal from contaminated water

Tasrina Rabia Choudhury [a,*], Md. Sajjad Hossain Sajib [b], Sheikh Fahim Faysal Sowrav [c], Shahidur R. Khan [a], M. Nur E. Alam [a], Md. Nurul Amin [b,*]

[a] Analytical Chemistry Laboratory, Chemistry Division, Atomic Energy Centre Dhaka, Bangladesh Atomic Energy Commission, Dhaka 1000, Bangladesh
[b] Department of Applied Chemistry and Chemical Engineering, University of Dhaka, Dhaka 1000, Bangladesh
[c] Department of Oceanography and Hydrography, Bangabandhu Sheikh Mujibur Rahman Maritime University, Bangladesh

A B S T R A C T

Possessing variable valence states, the element Arsenic (As) is intimidating the quality of the ecology and human health severely. In this study, eliminating As (III) from water-based solutions with great efficiency was done using Bagasse-Mn-Al, a sugarcane bagasse-derived biochar impregnated with Mn and Al. The Bagasse-Mn-Al composite yielded higher removal efficiency towards As (III) than the biochar itself. About 89.53 % of As (III) was removed within 65 min maintaining the very first concentration of As (III) at 400 μg/L, initial pH at 2–2.5, and adsorbent dosage at 0.625 g/L. The Bagasse-Mn-Al composite showed an adsorption potential maximum of 54.945 mg/g which is superior to most of the cheaply synthesized metal-impregnated biochar reported. Results from a variety of characterization techniques indicated that the •OH free radical in the Bagasse-Mn-Al composite mainly contributed to the removal of As (III) where oxidation and complexation were the major mechanisms. With high catalytic efficiency, this cost effectively produced metal-coated biochar showed easy and effective separation of As (III) from aqueous solution. Further, this study focuses on the high potential of Bagasse-Mn-Al adsorbent in the treatment of both ground and wastewater.

1. Introduction

Water, often hailed as the essence of life on Earth, possesses remarkable properties that sustain ecosystems and support all living organisms. As the universal solvent, water has the unique ability to dissolve a wide range of substances, making it essential for transporting nutrients, facilitating chemical reactions, and maintaining the balance of ecosystems. Water, with its remarkable ability to dissolve almost anything, assumes a dual role in our world—both as a guardian of life and as a potential harbinger of danger. Water, unfortunately, can become contaminated during its journey through various applications and processes. Contaminated water from various manufacturing processes consists of both inorganic and organic substances. Especially the heavy metals in it have raised concerns among the community and have forced extensive research on it. According to the United States Environmental Protection Agency (EPA), all the heavy metals e.g., arsenic, mercury, chromium, lead, and cadmium are the most threatening [1–4]. Also, the World Health Organization (WHO) is conducting regular assessments on the impact of contaminated drinking water on human health. Studies have found that among the toxic heavy metals, arsenic shows the most negative and chronic effects [5].

Arsenic is prevalent in water both in inorganic and organic forms. The organic form includes methyl and dimethyl derivatives of arsenic compounds. Whereas inorganic arsenic exists in Arsenite (As (III)) and arsenate (As (V)) form. As (III) is prevalent as H_3AsO_3, $H_2AsO_3^-$, and $HAsO_3^{2-}$, where As(V) as H_3AsO_4, $H_2AsO_4^-$, and $HAsO_4^{2-}$ [6,7]. Anthropogenic pathways like excessive groundwater extraction, chemical pesticides, ceramic manufacturing, and petroleum refining industries as well as mine wastes can produce arsenic-contaminated water. Also, natural phenomena such as soil erosion, weathering, and volcanic eruption play a pivotal role in this regard [8]. The inorganic form shows more toxicity than the organic form of arsenic. The As (III) forms are more thermodynamically stable and mobile and hence show more severity in terms of toxicity. Prolonged exposure to As (III) causes arsenicosis, diabetes, cancer (lung, skin, kidney, liver, and bladder), cardiovascular diseases, and neurological effects [9–11]. A Study found arsenic content of 13.2 mg/kg and < 3 mg/kg in arsenic patients and normal people respectively [12]. For this reason, the WHO as well as the EPA has set the threshold limit of As in drinking water at a range from 50 μg/L to 10 μg/L [1,5]. But this limit can vary with countries. For Bangladesh, the national standard of As for drinking water is 50 μg/L. The presence of arsenic was first observed in 1993 in the country. Groundwater from tubewells in 62 districts out of 64 here is contaminated with arsenic [13]. Studies have found that about 29 % of water

* Corresponding authors.
E-mail addresses: tasrina.rabia@gmail.com (T.R. Choudhury), namin@du.ac.bd (Md.N. Amin).

https://doi.org/10.1016/j.enceco.2024.09.002
Received 18 May 2024; Received in revised form 19 August 2024; Accepted 27 September 2024
Available online 30 September 2024

from tubewells in Bangladesh is contaminated with arsenic content over the national standard (50 μg/L) [14]. Water from most of the tubewells contaminated with As has contamination ranging from 100 μg/L to 300 μg/L with the highest detection of 4.7 mg/L [15]. Not only through drinking water but also through consumption of food, arsenic is affecting millions of Bangladeshis [16]. Contaminated water with arsenic is utilized for irrigating purposes and this helps in the accumulation of arsenic in food stuffs. Studies revealed that Bangladeshi rice contained an average of 0.1 to 0.95 μg/g of arsenic [17]. Hence extensive research on arsenic removal from ground and waste water is a crying need for this country.

Various methods have been developed over the years such as exchange of ions [18], chemical precipitation [19], membrane technologies [20], reverse osmosis [21], and electrochemical treatment [22]. But often these methods find restrictions in application for complexity and high cost. Adsorption on the other side is comparatively cheaper, simpler, and also highly efficient in the removal of As (III) and As (V) [23,24]. Large surface area, various surface groups, regeneration of adsorbent after use, and less toxic sludge generation have made the adsorption process really attractive. Previous works on the removal of arsenic have been based on activated carbon [25,26], activated alumina [27], hydrous zirconium oxide [28,29], lanthanum-loaded silica gel [30], titanium oxides [31] and metal oxides (magnetite, hematite, goethite, and ferrites) [32–35]. Among them, activated carbon and ion-exchange resin are globally used for adsorption purposes. However, they find limited application in developing nations because of the high cost and operational complexities [36].

The use of biosorbent prepared from agro-waste can be a cheaper option and also useful as it utilizes the waste and thus reduces the emissions from waste management. There have been studies on the removal of arsenic using biosorbents including duckweed, neem bark, and sawdust [37,38]. There have also been studies on activated carbon from biowastes impregnated with a variety of chemical agents to remove arsenic. But those required a pre-oxidation of As (III) to As (V) made the process more complex and uneconomical. Oxides of transitional metals such as Fe, Ti, Zr, Mn, and Cu are reported to oxidize as well as adsorb As (III) and As (V) and thus can reduce the complexity of pre-oxidation with resulting side effects [39–42]. Also composite of bimetals has shown to be more effective due to synergistic effects. Fe—Mn bimetal oxide [43], Zr—Mn bimetal oxide [44], Ce—Ti bimetal oxide [31], Ce—Mn bimetal oxide [45], Fe—Ni bimetal oxide [46] have shown high efficiency in terms of arsenic uptake from water. Also, there has been a satisfactory outcome on the use of tri-metal oxide composite. Effective elimination of As (III) and As (V) by Fe-Ni-Mn tri-metal oxide [47], Al-Ti-Mn tri-metal oxide [48], Fe-Ti-Mn tri-metal oxide [49], and Co-Al-Fe tri-metal oxide [50] were sighted. Furthermore, the use of tri-metal oxide-impregnated biochar in arsenic removal has shown high prospects. Fe-Mn-La-impregnated biochar has been reported to remove As (III) effectively [51]. Therefore, based on the previous works, the attempt of arsenic removal using bimetallic biochar prepared from agricultural wastes has been introduced in this study. Developed biochar based on Al (aluminium) and Mn (manganese) have been widely used for water treatment application due to low manufacturing cost and high removal efficiency. Until recently, aluminium was considered harmless for the human organism as it is readily excreted through urine. However, studies of environmental toxicology conducted in recent years indicated that aluminium could be a cause of many diseases in humans, animals and plants. At elevated exposures, Mn has been associated with increased levels of externalizing behaviors, including irritability, aggression, and impulsivity. Moreover, there is no available data regarding potential interactions between exposure to Mn and other metals, especially arsenic (As).This study will help in achieving the Sustainable Development Goals (SDG- 3,6 and 14) Bangladesh is aiming to achieve by 2030 [52].

Hence this research focuses on the (1) synthesis of the metal-impregnated biochar (2) characterization of the biochar composite using a variety of techniques (3) evaluation of its efficacy on the removal of As from ground and wastewater in both high and low-level concentration and (4) possible removal mechanism of the adsorbent.

2. Materials and methods

2.1. Chemicals and reagents

All the chemicals utilized in this research were of analytical grade. $Al_2(SO4)_3.18H_2O$ and $KMnO_4$ were taken for chemical activation of the biochar prepared from sugarcane bagasse. 1000 mg/L standard solution of Arsenic (III) (Spectro Pure, USA) was used to prepare different concentrations of As (III) solution by dilution. Highly purified Milli-Q water (water resistivity >18.2 MΩ-cm, 25 °C; Millipore, MA, USA) used for dilution purposes. NaOH and HNO_3 were used for pH adjustment of the As (III) solution.

2.2. Synthesis of B-Mn-Al adsorbent

The sugarcane used in the present work was collected from a local farm. After harvest, the residual sugarcane was weathered (for 10 days) till the moisture content constant was reached. The collected materials were washed with DI water several times to remove dust and fines. The washing process was repeated until the color of the wash water was transparent. The washed materials were then dried in a hot-air oven at 105 °C for 24 h. The bagasse was then powdered using a grinder and sieved to obtain a homogenized powder. This powdered raw material was then placed into crucibles with lids on it and then placed into a muffle furnace. In the furnace, it was subjected to slow pyrolysis at 500 °C for 2 h. The obtained biochar was then taken out of the furnace when it was conveniently cooled. Biochar obtained from bagasse was 1.3799 g. It was then impregnated with manganese and aluminium metals by the coprecipitation method [53]. For this purpose, biochar and salts were taken maintaining a biochar-to-salt ratio of 1:1. Among the salts, 0.23 g of $Al_2(SO4)_3.18H_2O$ and 0.23 g of $KMnO_4$ were added in 100 mL of water. After the salts were completely dissolved, 0.46 g of biochar was added and stirred using a glass rod. After some period of aging at room temperature, this mixture was magnetically agitated for 2 h. It was then filtered using a vacuum filter. The filter cake was washed with DI water so that excess chemicals were removed. The obtained filter cake was then dried in an oven for 2 h. When it is completely dried, it is further placed into the muffle furnace for chemical activation of the biochar. There it was kept at 700 °C for 1 h. Finally, 0.895 g of B-Mn-Al activated carbon was obtained through this process. It was then stored for further application.

2.3. Characterization of materials

Scanning Electron Microscope(SEM) (JEOL, USA) was used to observe the morphology of the adsorbent surface, its pores, cracks and image was captured at 10,000× and 5000 × magnification and 7.2 mm working distance at vacuum mode with 5.00Kv [54]. Energy Dispersive X-ray (EDS) was utilized for the elemental composition of the impregnated Mn and Al as well as the adsorbed As on the adsorbent surface. XRD (X-Ray Diffraction) was used to identify the crystallinity, purity, and adsorbed metals [55]. XRD analysis was done with Ultima IV, Rigaku Corporation at 40 kV and 40 mA. Cu K α radiation with a wavelength of 1.54 Å was utilized for the X-ray diffraction analysis, and the samples were securely positioned in a glass holder.

2.4. The scanning

Process was conducted from 20°to 100° at a rate of 3.0 deg./min. Fourier Transform Infrared spectroscopy (FTIR,8400S Shimadzu, Japan) was adopted to inspect the presence of functional groups involved in adsorption as well as the change in their peaks of to predict the

adsorption kinetics whether it is chemisorption or not. pH meter (HANNA Instrument,HI-98107, Germany) was used to adjust the pH of the As (III) solution during the experiment. To analyze the content of As (III) present in the sample, AAS (Atomic Absorption Spectroscopy) was done using (Varian AA240, USA) at the Analytical Chemistry Laboratory, Chemistry Division, Atomic Energy Centre, Dhaka, Bangladesh.

2.5. Adsorption experiment

To find out an optimum dosage of the adsorbent to start with, 0.02 g, 0.04 g, 0.05 g, 0.07 g, and 0.11 g of the adsorbent were taken and placed at the bottom of five adsorption columns. Then 80 mL of As (III) solution at pH 3.5 with an initial concentration of 500 µg/L was poured into each of these columns. Adjusting the flow rate, these solutions were allowed to percolate through the adsorbent for a period of 120 min. From here 0.05 g adsorbent was selected for further analysis. Then the pH was varied for choosing a suitable one. With the initial concentration of 500 ppb, As (III) solutions of pH 2, pH 4, pH 7, and pH 9 were prepared and 80 mL of each of them were allowed to percolate through 0.05 g of adsorbents in each of the columns for 65 min. The analytic report showed maximum removal efficiency for pH ~ 2. From here, selecting the dosage of 0.05 g adsorbent (0.625 g/L), As (III) solution of pH 2, and a contact time of 65 min, the concentration of the solution was modified to determine the most favorable concentration. Here solution of 50 µg/L, 500 µg/L, 800 µg/L, 1200 µg/L and 1700 µg/L were used for analysis. The optimum result was obtained for the solution of 500 µg/L. And last of all, time was varied for 40 min, 55 min, 65 min, 80 min, 95 min, and 110 min considering all the other parameters constant. It was shown that maximum removal of As (III) was obtained for a contact time of 65 min. Finally, results obtained from the above four steps were combined and an adsorbent dosage of 0.625 g/L, pH of the As (III) solution at 2, the initial concentration at 500 µg/L and contact time of 65 min was selected for further analysis.

3. Results and discussion

3.1. Comprehensive characterization of biochar composite

3.1.1. FTIR analysis

The presence of chemical bonds in a sample can be detected using Fourier-transform infrared spectroscopy (FTIR) analysis. This technique allows us to predict the mechanism of adsorption by identifying the functional groups on the adsorbent surface and observing how they change before and after the adsorption process.

In this study, FTIR was performed to identify the functional groups present on the adsorbent surface and their transformations during adsorption. This information was crucial in predicting whether the adsorption mechanism involved chemisorption. Three major peaks were observed at 3223.93 cm^{-1}, 1571.22 cm^{-1} and 1072.07 cm^{-1} from the FTIR analysis of the adsorbent before adsorption. After adsorption, three peaks were found at 3216.21 cm^{-1}, 1577.84 cm^{-1} and 1059.28 cm^{-1}. The FTIR spectra of the adsorbent before and after adsorption of As(III) are shown in Fig. 1.

The absorption band at 3223.93 cm^{-1} corresponds to the stretching vibration of hydroxyl groups (–OH). After the adsorption of As(III), this peak shifted to 3216.21 cm^{-1}, indicating the involvement of hydroxyl groups in the adsorption process. This shift suggests a high affinity and participation of the –OH group in forming a stable complex with As(III). The interactions that may occur are described by the following equation, as per references [56,57]:

$$\text{Biochar} - \text{MeOH} + H_2AsO_3^- \leftrightarrow \text{Biochar} - \text{MeHAsO}_3^- + H_2O \ (\text{Me} = \text{Mn, Al})$$

There might be hydrogen bonding between the –OH group and arsenate ions, as suggested by [56,57].

The other two peaks at 1577.84 $cm^{-1}$and 1059.28 cm^{-1} correspond to C═O and C—O groups, respectively [58,59]. The shift of peaks from 1571.22 cm^{-1} to 1577.84 $cm^{-1}$and from 1072.07 cm^{-1} to 1059.28 cm^{-1} indicates the involvement of these functional groups in the adsorption of As(III). Furthermore, the decrease in transmittance of the peaks in Fig. 1 suggests the adsorption of As(III).Considering the obtained FTIR data, it is possible to suggest that the adsorption process exhibits characteristics of chemisorption. This conclusion is supported by the pseudo second-order kinetics adsorption model.

3.1.2. SEM-EDS analysis

In this study, SEM analysis was done to inspect the surface morphology of the synthesized activated carbon (B-Mn-Al). The obtained SEM image of activated carbon before and after adsorption is shown in Fig. 2(a,b) and Fig. 2(c,d) respectively. A porous surface with spherical particles is shown in Fig. 2(a) and Fig. 2(b). These spherical particles might be the Mn and Al metals that were impregnated. EDS analysis further confirmed it. It showed the successful impregnation of Mn and Al metals on the biochar. EDS analysis report from Fig. 2(f)

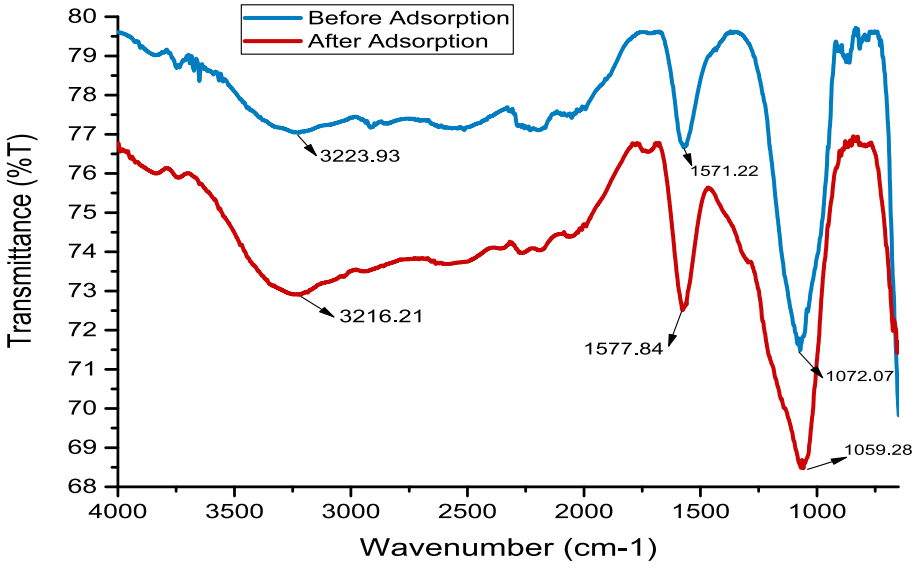

Fig. 1. FTIR spectra of adsorbent before and after adsorption.

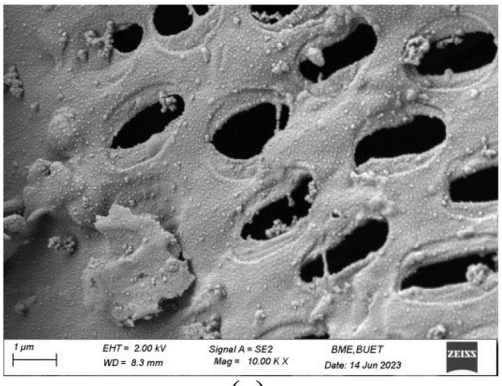

(a)

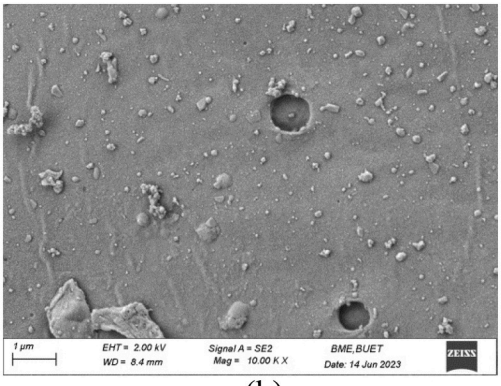

(b)

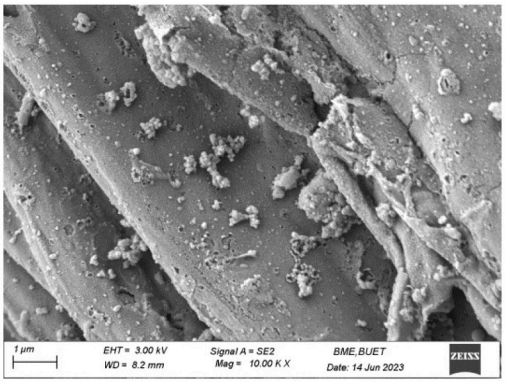

(c)

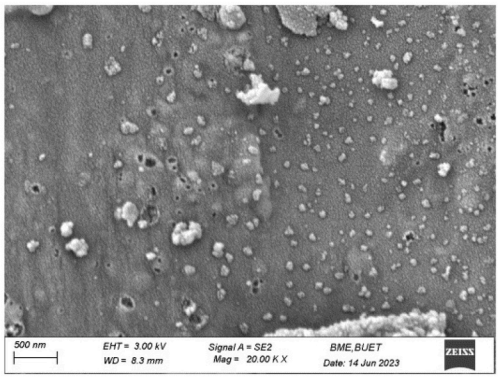

(d)

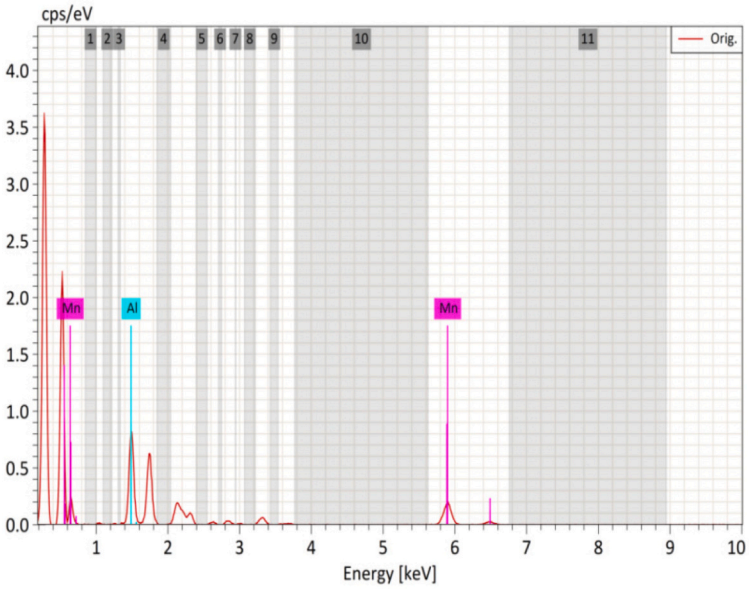

(e)

Element	At. No.	Netto	Mass [%]	Mass Norm. [%]	Atom [%]	abs. error [%] (3 sigma)
Al	13	67132	6.12	17.64	30.37	0.62
Mn	25	29697	28.58	82.36	69.63	3.10
		Sum	**34.70**	**100.00**	**100.00**	

(f)

Fig. 2. SEM analysis of adsorbent before adsorption 2(a,b) and after adsorption 2(c,d), and EDS analysis of adsorbent before adsorption 2(e,f) and after adsorption 2 (g,h).

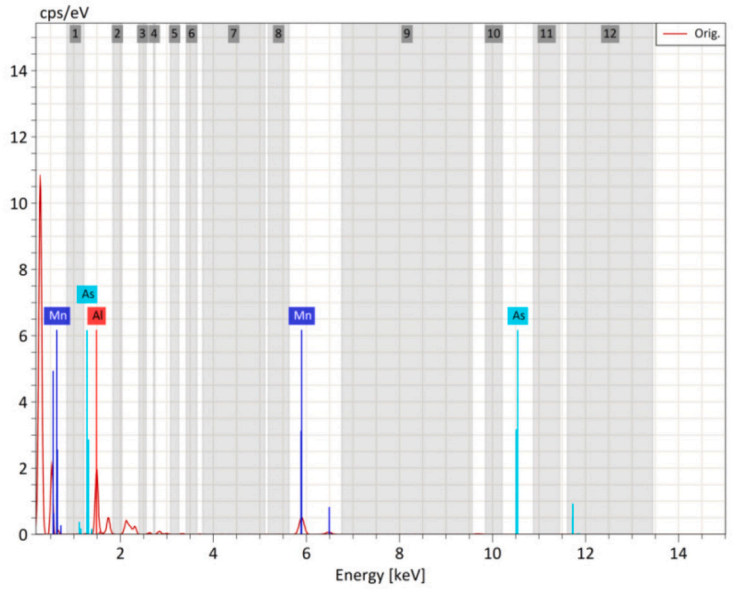

(g)

Element	At. No.	Netto	Mass [%]	Mass Norm. [%]	Atom [%]	abs. error [%] (3 sigma)
Al	13	100189	5.41	29.63	46.21	0.55
Mn	25	50356	12.75	69.87	53.51	0.82
As	33	1010	0.09	0.50	0.28	0.05
		Sum	**18.26**	**100.00**	**100.00**	

(h)

Fig. 2. (*continued*).

revealed that 34.70 wt% of the activated carbon was metal of which 6.12 % constitutes Al and 28.58 % is Mn. In Fig. 2(c,d), a comparatively dense surface is observed. This may be due to the fact that after the adsorption of As (III), the surface gets more filled with spherical particles. And because of the smaller gaps of the adsorbed particles, aggregates are found which has made the surface more dense. These aggregates in Fig. 2(c,d) might be of arsenic. The EDS report further confirms it. It is revealed from Fig. 2(h) that 18.26 wt% of the activated carbon is metal of which 0.09 wt% is As. The concentration of As (III) before and after adsorption can also be predicted from the EDS peak intensity. A higher intensity in the peaks corresponds to a higher concentration of the adsorbed metal. EDS peak from Fig. 2(e) and Fig. 2(g) shows a high cps/ev of As after adsorption. This corresponds to a good concentration of As(III). So it clearly shows that a good proportion of As (III) is adsorbed using the B-Mn-Al adsorbent. This makes the synthesized Mn and Al-impregnated biochar a possible one for the As (III) removal from the aqueous medium.

3.1.3. XRD analysis

XRD (X-ray diffraction) spectra of the synthesized adsorbent were analyzed and compared to identify the crystalline character, presence of impregnated metals, and purity of the adsorbent. In Fig. 3(a), 6 broad peaks were found at 2Θ values of 32.60°, 36.05°, 38.02°, 44.40°, 60.25° and 64.43°. Broad peaks suggest the amorphous structure of the sample. The distinct peaks indicate the presence of Mn and Al as Aluminium Manganese (Al_6Mn) according to DB Card no. 01–087-1521. Thus it shows the accomplished insemination of Mn and Al on the surface of the biochar supporting the results from EDS analysis. There was also the absence of foreign peaks except the peak at 2Θ of 32.60°. This indicates the high purity of the synthesized adsorbent. From Fig. 3(b), 4 peaks at 2Θ values of 36.24°, 44.31°, 58.06° and 64.67° corresponding to phase plane (111), (112), (004) and (104) were observed respectively. The absence of a foreign peak indicates the high purity of the sample here. It also verifies the successful adsorption of As as Manganese Arsenide (Mn_2As) on the surface according to DB Card no. 03–065-2262.

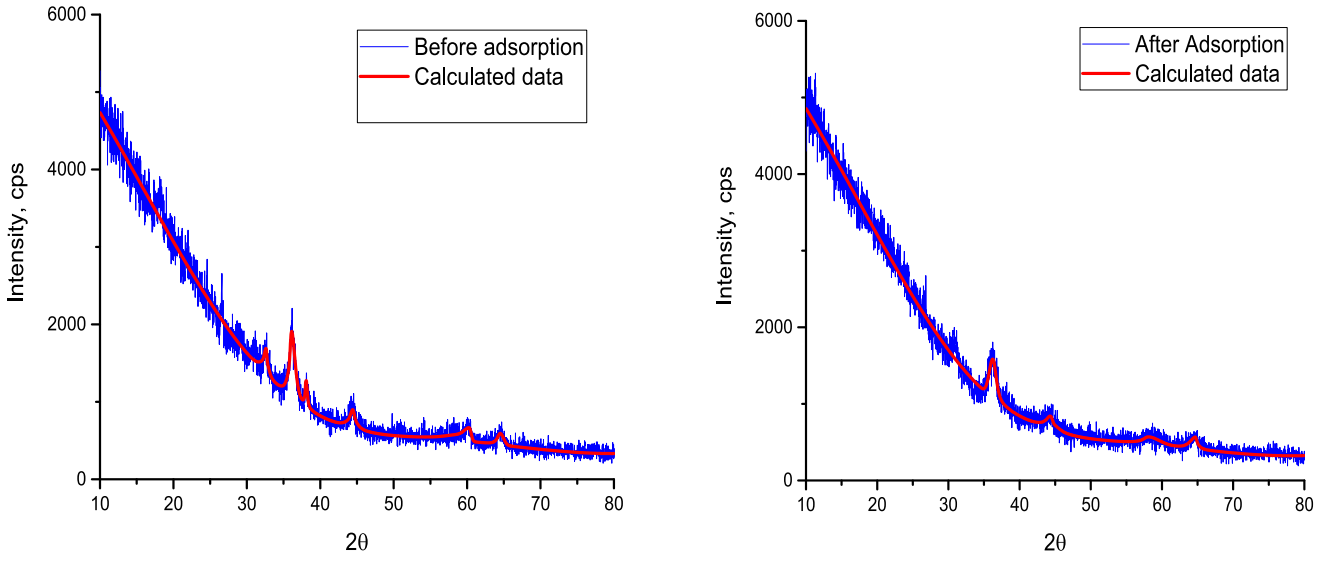

Fig. 3. XRD spectra of B-Mn-Al (a)before adsorption and (b) after adsorption.

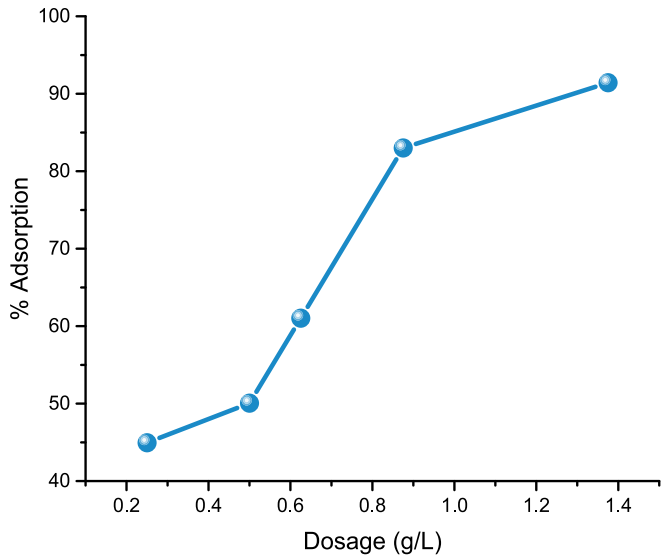

Fig. 4. Effect of adsorbent dosage on As (III) adsorption.

3.2. Batch adsorption studies

3.2.1. Effect of the dosage of adsorbent on adsorption

Increasing the dosage of adsorbent has a significant impact on the removal of As (III). From Fig. 4 it is observed that increasing adsorbent dosage increases the removal efficiency of As (III). Maintaining a contact time of 65 min, % Adsorption of As (III) jumped from 44.96 % at an adsorbent dosage of 0.25 g/L to 91.43 % at a dosage of 1.375 g/L adsorbent. The reason behind this can be elucidated by the fact that as the dosage of adsorbent increases, the quantity of active sites accessible for the adsorption of As (III) also escalates.

3.2.2. Effects of pH on adsorption

The pH value of the aqueous solution containing As (III) has a direct effect on the process of adsorption, as it not only governs the surface charge of the adsorbent but also impacts the extent of ionization of As (III). The results obtained from the investigation on the impact of pH on the removal of As (III) from the aqueous medium are depicted in Fig. 5. It was also observed that the % Adsorption of As (III) followed a downturn with increasing pH value. The highest level of adsorption, amounting to 88.85 %, was attained when the solution had a pH of 2 and a duration of contact of 65 min. At lower pH levels, the protonation of biochar surface groups is favored, resulting in a positively charged surface. This positively charged biochar enhances the adsorption capacity for arsenic (As) anions. Conversely, at higher pH levels, the biochar surface becomes negatively charged, repelling As anions and reducing adsorption efficiency.

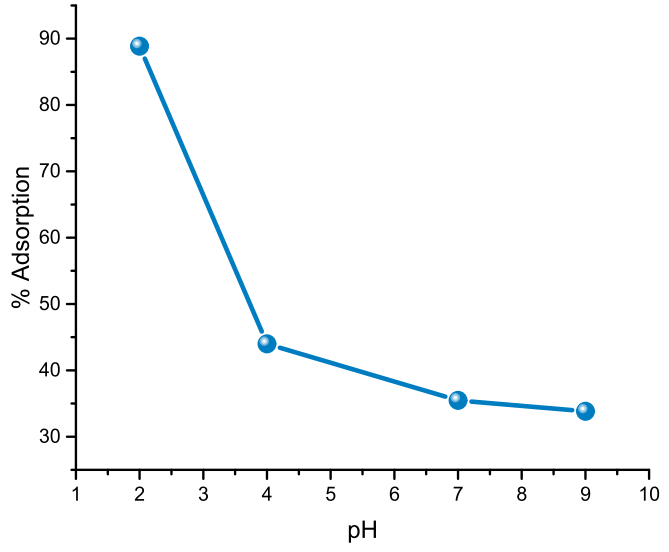

Fig. 5. Effect of pH of the solution on As (III) adsorption.

As the solution pH increased from 2 to 9, the redox reaction between As(III) and manganese (Mn) oxides was suppressed, leading to a noticeable decrease in As(III) removal. Thus, the efficient removal of As (III) at low pH can be attributed to the high reactivity of Mn oxides and the predominant role of oxidation effects.

The adsorption percentage of As(III) showed a diminishing pattern, increasing from 35.48 % at pH 7 to 33.84 % at pH 9. This trend can be explained by the positive charge of the adsorbent surface at lower pH levels. Protonation of surface –OH groups makes the surface gradually more positive as the pH decreases. Additionally, the arsenate ion formed by the oxidation of As(III) predominates as $HAsO_4^-$ and $HAsO_4^{2-}$ in acidic media. These negatively charged ions are more attracted to the positive surface of the adsorbent, enhancing physical sorption.

As the pH increases, deprotonation occurs, resulting in a progressively negative surface on the adsorbent. At pH 7, As(III) exists primarily as H_3AsO_3, which adsorbs mainly through physical sorption. Further increases in pH make the surface more negative, ultimately inhibiting the approach of arsenic anions to the adsorption sites due to electrostatic repulsion. This explains the observed declining trend in adsorption efficiency with increasing pH.

3.2.3. Effect of initial arsenic concentration on adsorption

The study showed a noteworthy result regarding the influence of initial concentration of As (III) solution on the removal efficiency. According to the study, it was determined that the adsorption of As(III) increased up to a certain point as the concentration increased. But beyond that point, further increasing of concentration affected adversely. Results shown in Fig.S1 revealed that % adsorption leaped from 73.205 % with an initial concentration of 31.76 μg/L to 88.851 % with that of 496 μg/L. A downturn was observed after further increasing of initial concentration beyond this point with the lowest %adsorption of 33.97 % observed at 1681 μg/L. Now this incident can be explained by the fact that the ratio of the number of available adsorption sites to the number of adsorbate molecules is quite large at a lower concentration of As (III). With the increasing of initial concentration, the number of As (III) molecules gets increased, but the available adsorption sites remained the same. Hence with increasing concentration, this ratio of the number of active adsorption sites to that of the adsorbate molecule gets decreased. This is why such a declining pattern of the % adsorption is observed with increasing initial concentration after attaining the maximum point.

3.2.4. Effect of time on adsorption

The passage elucidates the notable influence of time on the elimination of As (III) from a solution composed of water. In order to validate this assertion, the process of adsorption was permitted to occur at specific time intervals spanning 40, 55, 65, 80, 95, and 110 min. From Fig. S2 it is observed that the removal efficiency increases very rapidly during the first 60 min of adsorption. But beyond that the process gets slower and achieves an equilibrium condition gradually. The study showed that the %adsorption jumped rapidly from 82.02 % at 40 min to 89.526 % at a time interval of 65 min. After that, up to a time interval of 110 min, the process reached equilibrium with a % adsorption of 89 % more or less. This phenomenon observed can be explained by the fact that at the beginning of the process, there is abundance of adsorption sites. With increasing time, the number of adsorption sites decreased and hence the removal process gets slower. When all the available adsorption sites are blocked, the process finally gets the equilibrium condition. This is why 65 min time interval was chosen as the contact time for

further analysis.

3.3. Mechanism of adsorption

Adsorption of As (III) on B-Mn-Al adsorbent surface is thought to occur in two routes. One is electrostatic adsorption and the other one is through ion or ligand exchange between the adsorbate arsenate ion and the active functional groups on the adsorbent surface. Electrostatic adsorption is a physical adsorption that is linked with the surface behavior of the sugarcane bagasse. Impregnated Al and Mn metal existed as their oxides which ultimately converted into –OH groups. These layer of –OH groups presented an increased number of active sites. The Mn—O moieties might oxidize the As (III) to As (V). The EDS report supports the participation of Mn in the adsorption. From Fig. 2(f) and 2 (h), it could be seen that there was a decrease in the Atomic % of Mn. This suggests that there might be a reaction between Mn and As that triggered the release of Mn-containing species. XRD data further revealed the adsorption of Arsenic as Manganese arsenide (Mn_2As)on the surface. In this way, promoting oxidation, Mn might have facilitated the As (III) adsorption as As (V) could be removed more readily than As (III). Al-OH moieties might be involved with ion exchange with the arsenate ions in the solution. The decrease in atomic% of Al according to Fig. 2 (f) and Fig. 2 (h) might be due to the participation of Al in arsenic adsorption. In acidic conditions there might be reactions like the following,

Biochar-AlOH + $HAsO_4^{2-}$ ↔Biochar-$AlAsO_4$ + H_2O [60].

The red shifts of FTIR peaks suggested the involvement of the functional groups. These functional groups might took part in complex formation with the As at the surface of the adsorbent. So it can be summed up that the adsorption process went through oxidation, ion or ligand exchange besides physical adsorption.

3.4. Adsorption kinetics

A study was conducted to investigate the kinetics of sorption of As (III) on B-Mn-Al adsorbent using pseudo first order and pseudo second order kinetics. The experimental data was used to understand the sorption kinetics. The linear form of the kinetic models, namely the pseudo-first order and pseudo-second order, can be expressed by the equations provided:

$$ln(q_e - q_t) = lnq_e - K_1 t \quad (1)$$

$$\frac{t}{q_t} = \frac{1}{K_2 q_e^2} + \frac{t}{q_e} \quad (2)$$

Using eq. (1) and (2) for pseudo first order and pseudo-second order kinetics respectively, ln (q_e-q_t) against t and t/q_t against t graphs were plotted in Origin pro 2016. The obtained values of different kinetic parameters are enlisted in Table 1. Among the kinetics model parameters, q_t (mg/g) is the adsorption capacity of the adsorbent at time t, K_1(min^{-1}) and K_2($g.mg^{-1}.min^{-1}$) indicates the rate constant for pseudo first order and pseudo second order kinetics respectively, q_e is the maximum adsorption capacity of the adsorbent at equilibrium, and R^2 is the regression coefficient. Analyzing the obtained values and Fig. S3(b), it was found that the data were best fitted with pseudo second order kinetics since the theoretical q_e value obtained from this model is nearer to the experimental q_e. The regression coefficient (R^2 = 0.9986) value also supports the pseudo second-order kinetic model. Further it is quite lucid from Fig. S3(a) that the pseudo first order kinetics model didn't fit well at all. Hence this implies that the adsorption process follows chemisorption according to the pseudo second-order kinetics model.

Table 1
Kinetic parameters for Pseudo first-order, pseudo second-order models for the adsorption of As(III).

Kinetics model	Parameters	Values
Pseudo first order	K_1	0.06153
	q_e*(mg/g)	0.573
	R^2	0.80145
	q_e**(mg/g)	0.4265
Pseudo second order	K_2	0.38641
	q_e**(mg/g)	0.59855
	R^2	0.9986

*Experimental value, **Theoretical values.

3.5. Adsorption isotherms

The equilibrium between the adsorbate in solution and on the surface of the adsorbent was considered. An equilibrium isotherm study was conducted to predict the adsorption mechanism and maximum capacity for As (III) adsorption. The adsorption capacity was determined using eq. (3):

$$q_e = \frac{V}{m}(C_\circ - C_e) \quad (3)$$

Here, qe represents the adsorption capacity of the adsorbent at equilibrium, measured in milligrams per liter (mg/L). V denotes the volume of the solution, which is measured in liters (L). m represents the quantity of adsorbent used, measured in grams (g). $C_\circ$ indicates the initial concentration of As (III) in the solution, measured in milligrams per liter (mg/L). Ce represents the equilibrium concentration of As (III) in the solution, also measured in milligrams per liter (mg/L). Among the various isotherm models commonly utilized, the Langmuir and Freundlich isotherm models were taken into consideration. These isotherm models enable the prediction of the adsorption behavior in a solid-liquid system. The Langmuir isotherm model specifically supports the concept of monolayer adsorption, while the Freundlich isotherm model suggests the occurrence of non-uniform multilayer adsorption on the surface of the adsorbent. The data obtained from this study was used to fit the two models.

$$\frac{1}{q_e} = \frac{1}{k_L q_{max} C_e} + \frac{1}{q_{max}} \quad (4)$$

$$logq_e = logk_f + \frac{1}{n} logC_e \quad (5)$$

Here, q_{max} represents the upper limit of adsorption capacity possessed by the adsorbent (in milligrams per liter). K_L denotes the Langmuir adsorption constant (in liters per milligram), which offers insights into the affinity of the adsorbate towards the binding sites. K_f and n, on the other hand, correspond to the Freundlich empirical constants, which serve to estimate the strength of adsorption and the heterogeneity of the surface.

Linear forms of Langmuir and Freundlich isotherm model were plotted using eq. (4) and (5) respectively in Origin Pro 2016. Fig.S4(a) and Fig. S4(b) correspond to the Langmuir and Freundlich isotherm models, respectively. The values of the correlation coefficient (R^2) and other parameters for the equilibrium models are listed in Table 2. The data analysis shows that the correlation coefficient R^2 for the Langmuir isotherm (R^2 = 0.9827) is higher than that for the Freundlich isotherm (R^2 = 0.66275). Therefore, it is evident that the experimental data fits well with the Langmuir isotherm model, indicating that the As (III) removal process follows a monolayer homogeneous adsorption

Table 2
The values of Isotherms parameters of As (III) adsorption.

Langmuir isotherm Parameters	Values	Freundlich isotherm parameters	Values
Q_{max} (mg/g)	55.0964	1/n	0.60161
K_L	0.08052	K_f	1.31105
R_L	0.9616		
R^2	0.9827	R^2	0.66275

mechanism. Moreover, this suggests that all the adsorption sites are of equal importance. The K_L value ($K_L = 0.08052$) suggests good affinity of the adsorbate for the adsorbent. The R_L value indicates the nature of the adsorption whether it is favorable or not. A value less than 1 suggests that the adsorption is favorable, whereas, for 1 and greater than 1, the adsorption is linear and unfavorable respectively. In this study the R_L value of 0.9616 suggests that the process is quite favorable. Most important of all, from the Langmuir model, As (III) adsorption capacity of the adsorbent ($q_{max} = 55.0964$ mg/g) was calculated. Such value is significantly larger than the recently reported metal-impregnated biochar composites such as iron-oxide impregnated corn straw derived biochar ($q_m = 22.94$ mg/g) [61], Zn-loaded raw pine cone biochar ($q_m = 7$ mg/g) [62], BMN nanocomposites ($q_m = 16.23$ mg/g) [63], Magnetic calcium-rich biochar ($q_m = 15.8$ mg/g) [64], Hematite modified biochar ($q_m = 2.828$ mg/g) [65], Calcium based magnetic biochar ($q_m = 6.34$ mg/g) [66]. Adsorption capacity of pristine sugarcane bagasse biochar is reported 11.9 mg/g [67]. Therefore, the B-Mn-Al adsorbent can be so useful in removal of As (III) from aqueous medium in a cost-effective and non-hazardous way.

4. Conclusion

In this study, B-Mn-Al activated carbon was synthesized from a cost effective combination of biowaste (sugarcane bagasse), $Al_2(SO4)_3.18H_2O$, and $KMnO_4$ following a simple procedure. The activated carbon had a maximum adsorption capacity of 54.945 mg/g, which is higher than most biochar-derived adsorbents. This efficiency is due to the successful impregnation of Mn and Al, as confirmed by SEM-EDS, XRD, and FTIR analysis. The adsorption of As (III) was directly influenced by pH. Removal efficiency decreased with the increase of pH. Experimental data supported the pseudo second order kinetics that suggested chemisorption. The most probable mechanism for adsorption was electrostatic adsorption, oxidation, ion or ligand exchange and complexation. Also supporting the Langmuir isotherm model predicts the homogenized monolayer adsorption. In summary, the B-Mn-Al can efficiently remove As (III) from a very low concentration of aqueous solution which makes it a potential adsorbent for the treatment of As-polluted water.

CRediT authorship contribution statement

Tasrina Rabia Choudhury: Writing – review & editing, Validation, Supervision, Software, Project administration, Methodology, Investigation, Funding acquisition, Formal analysis, Data curation, Conceptualization. **Md. Sajjad Hossain Sajib:** Writing – original draft, Methodology, Investigation. **Sheikh Fahim Faysal Sowrav:** Data curation. **Shahidur R. Khan:** Methodology. **M. Nur E. Alam:** Writing – original draft, Methodology, Investigation. **Md. Nurul Amin:** Supervision, Conceptualization.

Declaration of competing interest

The authors declare that they have no known competing financial interests or personal relationships that could have appeared to influence the work reported in this paper.

Acknowledgements

The authors would like to acknowledge the Analytical Chemistry Laboratory (ISO 17025 Accredited Lab), Atomic Energy Centre Dhaka, Bangladesh Atomic Energy Commission for technical support during the sample preparation and analysis. This work was carried out with the aid of a grant from UNESCO-TWAS and the Swedish International Development Cooperation Agency (Sida). The views expressed herein do not necessarily represent those of UNESCO-TWAS, Sida or its Board of Governors.

Appendix A. Supplementary data

Supplementary data to this article can be found online at https://doi.org/10.1016/j.enceco.2024.09.002.

References

[1] U. Epa, United States environmental protection agency, Qual. Assur. Guid. Doc. Qual. Assur. Proj. Plan PM Ambient Air 2 (2001) 12.
[2] M. Nurnabi, S. Bhowmik, M.S. Rahman, T. Rabia Choudhury, A.J. Parsons, S. D. Young, Modification and application of Albizia lebbeck sawdust for the sorption of Lead(II) and copper(II) from aqueous solutions, Orient. J. Chem. 36 (04) (2020) 591–600, https://doi.org/10.13005/ojc/360401.
[3] S. Ahmed, et al., Synthesis and characterization of graphene oxide for removal of Cr(III) from tannery effluent, Desalin. Water Treat. 244 (2021) 201–211, https://doi.org/10.5004/dwt.2021.27895.
[4] S. Ahmed, T.R. Fatema-Tuj-zohra, M.Z. Alam Choudhury, M. Nurnabi, Adsorption of Cu(II) and Cd(II) with graphene based adsorbent: adsorption kinetics, isotherm and thermodynamic studies, Desalin. Water Treat. 285 (2023) 167–179, https://doi.org/10.5004/dwt.2023.29290.
[5] W. H. Organization, Organotins in drinking-water, World Health Organization, 2020.
[6] A. Basu, D. Saha, R. Saha, T. Ghosh, B. Saha, A review on sources, toxicity and remediation technologies for removing arsenic from drinking water, Res. Chem. Intermed. 40 (2) (2014) 447–485, https://doi.org/10.1007/s11164-012-1000-4.
[7] K.S.M. Abdul, S.S. Jayasinghe, E.P.S. Chandana, C. Jayasumana, P.M.C.S. De Silva, Arsenic and human health effects: a review, Environ. Toxicol. Pharmacol. 40 (3) (2015) 828–846.
[8] T.G. Asere, C.V. Stevens, G. Du Laing, Use of (modified) natural adsorbents for arsenic remediation: a review, Sci. Total Environ. 676 (2019) 706–720, https://doi.org/10.1016/j.scitotenv.2019.04.237.
[9] J.S. Uppal, Q. Zheng, X.C. Le, Arsenic in drinking water—recent examples and updates from Southeast Asia, Curr. Opin. Environ. Sci. Heal. 7 (2019) 126–135, https://doi.org/10.1016/j.coesh.2019.01.004.
[10] V.M. Nurchi, A. Buha Djordjevic, G. Crisponi, J. Alexander, G. Bjørklund, J. Aaseth, Arsenic toxicity: molecular targets and therapeutic agents, Biomolecules 10 (2) (2020), https://doi.org/10.3390/biom10020235.
[11] M. Ashrafizadeh, et al., (Nano) platforms in bladder cancer therapy: challenges and opportunities, Bioeng. Transl. Med. 8 (1) (2023) e10353.
[12] T. Rabia Choudhury, M. Ali, S. Ahmed Rahin, M. Ali, Trace elements in the hair of normal and chronic arsenism people, Glob. Adv. Res. J. Environ. Sci. Toxicol. 2 (7) (2013) 163–173.
[13] I. Ahmed, Rights, rivers and the quest for water commons: the case of Bangladesh, Springer, 2021.
[14] G. DPHE, Feasibility Report on Rural water Supply in Bangladesh, 2015, pp. 1–36.
[15] S.A. Ahmad, M.H. Khan, M. Haque, Arsenic contamination in groundwater in Bangladesh: implications and challenges for healthcare policy, Risk Manag. Healthc. Policy 11 (2018) 251–261, https://doi.org/10.2147/RMHP.S153188.
[16] M.S. Islam, et al., Arsenic in the foodstuffs: potential health appraisals in a developing country, Bangladesh, Environ. Sci. Pollut. Res. 30 (10) (2023) 26938–26951, https://doi.org/10.1007/s11356-022-24119-w.
[17] P.N. Williams, A.H. Price, A. Raab, S.A. Hossain, J. Feldmann, A.A. Meharg, Variation in arsenic speciation and concentration in Paddy Rice related to dietary exposure, Environ. Sci. Technol. 39 (15) (Aug. 2005) 5531–5540, https://doi.org/10.1021/es0502324.
[18] A. Dominguez-Ramos, et al., Arsenic removal from natural waters by adsorption or ion exchange: an environmental sustainability assessment, Ind. Eng. Chem. Res. 53 (49) (Dec. 2014) 18920–18927, https://doi.org/10.1021/ie4044345.
[19] M.J. González-Muñoz, M.A. Rodríguez, S. Luque, J.R. Álvarez, Recovery of heavy metals from metal industry waste waters by chemical precipitation and nanofiltration, Desalination 200 (1–3) (2006) 742–744, https://doi.org/10.1016/j.desal.2006.03.498.
[20] P.S. Sudilovskiy, G.G. Kagramanov, A.M. Trushin, V.A. Kolesnikov, Use of membranes for heavy metal cationic wastewater treatment: flotation and membrane filtration, Clean Techn. Environ. Policy 9 (3) (2007) 189–198, https://doi.org/10.1007/s10098-007-0086-7.
[21] A. Abejón, A. Garea, A. Irabien, Arsenic removal from drinking water by reverse osmosis: minimization of costs and energy consumption, Sep. Purif. Technol. 144 (2015) 46–53, https://doi.org/10.1016/j.seppur.2015.02.017.
[22] D. Syam Babu, P.V. Nidheesh, A review on electrochemical treatment of arsenic from aqueous medium, Chem. Eng. Commun. 208 (3) (Mar. 2021) 389–410, https://doi.org/10.1080/00986445.2020.1715956.
[23] L. Hao, M. Liu, N. Wang, G. Li, A critical review on arsenic removal from water using iron-based adsorbents, RSC Adv. 8 (69) (2018) 39545–39560, https://doi.org/10.1039/C8RA08512A.
[24] S. Alka, S. Shahir, N. Ibrahim, M.J. Ndejiko, D.-V.N. Vo, F.A. Manan, Arsenic removal technologies and future trends: a mini review, J. Clean. Prod. 278 (2021) 123805, https://doi.org/10.1016/j.jclepro.2020.123805.
[25] V. Nejadshafiee, M.R. Islami, Adsorption capacity of heavy metal ions using sultone-modified magnetic activated carbon as a bio-adsorbent, Mater. Sci. Eng. C 101 (2019) 42–52, https://doi.org/10.1016/j.msec.2019.03.081.
[26] M. Asadullah, I. Jahan, M.B. Ahmed, P. Adawiyah, N.H. Malek, M.S. Rahman, Preparation of microporous activated carbon and its modification for arsenic

removal from water, J. Ind. Eng. Chem. 20 (3) (2014) 887–896, https://doi.org/10.1016/j.jiec.2013.06.019.
[27] N. Dutta, A. Gupta, Development of arsenic removal unit with electrocoagulation and activated alumina sorption: field trial at rural West Bengal, India, J. Water Process Eng. 49 (2022) 103013, https://doi.org/10.1016/j.jwpe.2022.103013.
[28] B. Pan, et al., Acid and organic resistant nano-hydrated zirconium oxide (HZO)/polystyrene hybrid adsorbent for arsenic removal from water, Chem. Eng. J. 248 (2014) 290–296, https://doi.org/10.1016/j.cej.2014.02.093.
[29] B. Moraga, L. Toledo, L. Jelínek, J. Yañez, B. L. Rivas, and B. F. Urbano, "Copolymer–hydrous zirconium oxide hybrid microspheres for arsenic sorption," Water Res., vol. 166, p. 115044, 2019, doi: https://doi.org/10.1016/j.watres.2019.115044.
[30] M.R. Gandhi, S. Meenakshi, Preparation and characterization of La(III) encapsulated silica gel/chitosan composite and its metal uptake studies, J. Hazard. Mater. 203–204 (2012) 29–37, https://doi.org/10.1016/j.jhazmat.2011.11.062.
[31] Z. Li, S. Deng, G. Yu, J. Huang, V.C. Lim, As(V) and as(III) removal from water by a Ce–Ti oxide adsorbent: behavior and mechanism, Chem. Eng. J. 161 (1) (2010) 106–113, https://doi.org/10.1016/j.cej.2010.04.039.
[32] E. Di Iorio, et al., Characterization of magnetite nanoparticles synthetized from Fe(II)/nitrate solutions for arsenic removal from water, J. Environ. Chem. Eng. 7 (2) (2019) 102986, https://doi.org/10.1016/j.jece.2019.102986.
[33] C.B. Tabelin, R.D. Corpuz, T. Igarashi, M. Villacorte-Tabelin, M. Ito, N. Hiroyoshi, Hematite-catalysed scorodite formation as a novel arsenic immobilisation strategy under ambient conditions, Chemosphere 233 (2019) 946–953, https://doi.org/10.1016/j.chemosphere.2019.06.020.
[34] H. Basu, S. Singh, M. Venkatesh, M.V. Pimple, R.K. Singhal, Graphene oxide-MnO2-goethite microsphere impregnated alginate: a novel hybrid nanosorbent for As (III) and As (V) removal from groundwater, J. Water Process Eng. 42 (2021) 102129, https://doi.org/10.1016/j.jwpe.2021.102129.
[35] J. López-Luna, et al., Linear and nonlinear kinetic and isotherm adsorption models for arsenic removal by manganese ferrite nanoparticles, SN Appl. Sci. 1 (2019) 1–19.
[36] C. Duan, T. Ma, J. Wang, Y. Zhou, Removal of heavy metals from aqueous solution using carbon-based adsorbents: a review, J. Water Process Eng. 37 (2020) 101339, https://doi.org/10.1016/j.jwpe.2020.101339.
[37] T. Choudhury, T. Acher, M. Amin, S. Quraishi, A. Mustafa, Removal of arsenic (III) from groundwater by adsorption onto duckweed (Lemna minor), Int. Res. J. Pure Appl. Chem. 6 (3) (2015) 120–127, https://doi.org/10.9734/irjpac/2015/12798.
[38] T. Choudhury, Arsenic (III) removal from real-life groundwater by adsorption on neem bark (Azadirachta indica), Int. Res. J. Pure Appl. Chem. 4 (6) (2014) 594–604, https://doi.org/10.9734/irjpac/2014/2713.
[39] M.E. Pena, G.P. Korfiatis, M. Patel, L. Lippincott, X. Meng, Adsorption of as(V) and as(III) by nanocrystalline titanium dioxide, Water Res. 39 (11) (2005) 2327–2337, https://doi.org/10.1016/j.watres.2005.04.006.
[40] V. Lenoble, C. Laclautre, B. Serpaud, V. Deluchat, J.-C. Bollinger, As(V) retention and As(III) simultaneous oxidation and removal on a MnO2-loaded polystyrene resin, Sci. Total Environ. 326 (1) (2004) 197–207, https://doi.org/10.1016/j.scitotenv.2003.12.012.
[41] C.A. Martinson, K.J. Reddy, Adsorption of arsenic(III) and arsenic(V) by cupric oxide nanoparticles, J. Colloid Interface Sci. 336 (2) (2009) 406–411, https://doi.org/10.1016/j.jcis.2009.04.075.
[42] T.R. Choudhury, et al., Sythesis of Nano Zerovalent Iron supported sawdust (NZVI/SD) and its application for removal of arsenic (III) from aqueous solution, Chem. Sci. Int. J. 29 (1) (2020) 1–12, https://doi.org/10.9734/csji/2020/v29i130152.
[43] G. Zhang, J. Qu, H. Liu, R. Liu, R. Wu, Preparation and evaluation of a novel Fe–Mn binary oxide adsorbent for effective arsenite removal, Water Res. 41 (9) (2007) 1921–1928, https://doi.org/10.1016/j.watres.2007.02.009.
[44] G. Zhang, A. Khorshed, J. Paul Chen, Simultaneous removal of arsenate and arsenite by a nanostructured zirconium–manganese binary hydrous oxide: behavior and mechanism, J. Colloid Interface Sci. 397 (2013) 137–143, https://doi.org/10.1016/j.jcis.2012.11.056.
[45] J. Chen, J. Wang, G. Zhang, Q. Wu, D. Wang, Facile fabrication of nanostructured cerium-manganese binary oxide for enhanced arsenite removal from water, Chem. Eng. J. 334 (2018) 1518–1526, https://doi.org/10.1016/j.cej.2017.11.062.
[46] S. Liu, S. Kang, G. Wang, H. Zhao, W. Cai, Micro/nanostructured porous Fe–Ni binary oxide and its enhanced arsenic adsorption performances, J. Colloid Interface Sci. 458 (2015) 94–102, https://doi.org/10.1016/j.jcis.2015.07.038.
[47] A.M. Nasir, P.S. Goh, A.F. Ismail, Novel synergistic hydrous iron-nickel-manganese (HINM) trimetal oxide for hazardous arsenite removal, Chemosphere 200 (2018) 504–512, https://doi.org/10.1016/j.chemosphere.2018.02.126.
[48] D.N. Thanh, Z. Bastl, K. Černá, P. Ulbrich, J. Lederer, Amorphous nanosized Al–Ti–Mn trimetal hydrous oxides: synthesis, characterization and enhanced performance in arsenic removal, RSC Adv. 6 (103) (2016) 100732–100742, https://doi.org/10.1039/C6RA11347H.
[49] W. Zhang, et al., A novel nanostructured Fe-Ti-Mn composite oxide for highly efficient arsenic removal: preparation and performance evaluation, Colloids Surf. A Physicochem. Eng. Asp. 561 (2019) 364–372, https://doi.org/10.1016/j.colsurfa.2018.10.077.
[50] Y. K. Penke, G. Anantharaman, J. Ramkumar, and K. K. Kar, "Aluminum substituted cobalt ferrite (co−Al−Fe) Nano adsorbent for arsenic adsorption in aqueous systems and detailed redox behavior study with XPS," ACS Appl. Mater. Interfaces, vol. 9, no. 13, pp. 11587–11598, Apr. 2017, doi: https://doi.org/10.1021/acsami.6b16414.
[51] L. Lin, G. Zhang, X. Liu, Z.H. Khan, W. Qiu, Z. Song, Synthesis and adsorption of FeMnLa-impregnated biochar composite as an adsorbent for As(III) removal from aqueous solutions, Environ. Pollut. 247 (2019) 128–135, https://doi.org/10.1016/j.envpol.2019.01.044.
[52] "THE 17 GOALS | Sustainable Development.".
[53] L. Verma, J. Singh, Arsenic adsorption from aqueous solution and groundwater using monometallic (Fe) and bimetallic (Fe/Mn) Tectona biochar synthesized from plant refuse: mechanism, isotherm, and kinetic study, Environ. Eng. Res. 28 (3) (2022) 220110, https://doi.org/10.4491/eer.2022.110.
[54] S. Ahmed, T.R. Choudhury, M.Z. Alam, M. Nurnabi, Characterization and application of synthesized calcium alginate-graphene oxide for the removal of Cr3+, Cu2+ and Cd2+ ions from tannery effluents, Clean. Water 1 (Jun. 2024) 100016, https://doi.org/10.1016/J.CLWAT.2024.100016.
[55] T. R. Choudhury, F. N. Jahan, S. Bhowmik, S. F. F. Sowrav, and M. Nurnabi, "Enhanced chromium (VI) removal: a remediation study employing nano zero-valent iron supported by sawdust," Environ. Chem. Ecotoxicol., vol. 6, pp. 81–91, Jan. 2024, doi: https://doi.org/10.1016/J.ENCECO.2024.02.002.
[56] A.W. Samsuri, F. Sadegh-Zadeh, B.J. Seh-Bardan, Adsorption of as(III) and as(V) by Fe coated biochars and biochars produced from empty fruit bunch and rice husk, J. Environ. Chem. Eng. 1 (4) (2013) 981–988, https://doi.org/10.1016/j.jece.2013.08.009.
[57] M. Vithanage, I. Herath, S. Joseph, J. Bundschuh, Interaction of arsenic with biochar in soil Interaction of arsenic with biochar in soil and water: a critical review February (2018), https://doi.org/10.1016/j.carbon.2016.11.032.
[58] V.N. Van, M. Zafar, S.K. Behera, H. Park, Arsenic (III) Removal from Aqueous Solution by Raw and Zinc-loaded Pine Cone Biochar: Equilibrium, Kinetics and Thermodynamics Studies Arsenic (III) Removal from Aqueous Solution by raw and Zinc- Loaded Pine Cone Biochar: Equilibrium, Kinetics, A, no. April 2014, 2016, https://doi.org/10.1007/s13762-014-0507-1.
[59] S.A. Baig, J. Zhu, N. Muhammad, T. Sheng, X. Xu, Effect of synthesis methods on magnetic Kans grass biochar for enhanced As(III, V) adsorption from aqueous solutions, Biomass Bioenergy 71 (2014) 299–310.
[60] W. Zhang, J. Fu, G. Zhang, X. Zhang, Enhanced arsenate removal by novel Fe–La composite (hydr)oxides synthesized via coprecipitation, Chem. Eng. J. 251 (2014) 69–79, https://doi.org/10.1016/j.cej.2014.04.057.
[61] Z.H. Khan, M. Gao, W. Qiu, M. Qaswar, M.S. Islam, Z. Song, The sorbed mechanisms of engineering magnetic biochar composites on arsenic in aqueous solution, Environ. Sci. Pollut. Res. Int. 27 (33) (Nov. 2020) 41361–41371, https://doi.org/10.1007/s11356-020-10082-x.
[62] N. Van Vinh, M. Zafar, S.K. Behera, H.S. Park, Arsenic(III) removal from aqueous solution by raw and zinc-loaded pine cone biochar: equilibrium, kinetics, and thermodynamics studies, Int. J. Environ. Sci. Technol. 12 (4) (2015) 1283–1294, https://doi.org/10.1007/s13762-014-0507-1.
[63] J. Cui, Q. Jin, Y. Li, F. Li, Oxidation and removal of as(iii) from soil using novel magnetic nanocomposite derived from biomass waste, Environ. Sci. Nano 6 (2) (2019) 478–488, https://doi.org/10.1039/C8EN01257A.
[64] T. Chen, X. Quan, Z. Ji, X. Li, Y. Pei, Synthesis and characterization of a novel magnetic calcium-rich nanocomposite and its remediation behaviour for as(III) and Pb(II) co-contamination in aqueous systems, Sci. Total Environ. 706 (2020) 135122, https://doi.org/10.1016/j.scitotenv.2019.135122.
[65] S. Wang, et al., Removal of arsenic by magnetic biochar prepared from pinewood and natural hematite, Bioresour. Technol. 175 (2015) 391–395, https://doi.org/10.1016/j.biortech.2014.10.104.
[66] J. Wu, D. Huang, X. Liu, J. Meng, C. Tang, J. Xu, Remediation of as(III) and cd(II) co-contamination and its mechanism in aqueous systems by a novel calcium-based magnetic biochar, J. Hazard. Mater. 348 (2018) 10–19, https://doi.org/10.1016/j.jhazmat.2018.01.011.
[67] H. Tajernia, T. Ebadi, B. Nasernejad, M. Ghafori, Arsenic removal from water by sugarcane bagasse: an application of response surface methodology (RSM), Water Air Soil Pollut. 225 (7) (2014) 2028, https://doi.org/10.1007/s11270-014-2028-4.